Available online at www.sciencedirect.com
ScienceDirect
Physica D 237 (2008) 2101–2110
PHYSICA D
www.elsevier.com/locate/physd

Euler equations in geophysics and astrophysics

F.H. Busse*

Institute of Physics, University of Bayreuth, D-95440, Bayreuth, Germany

Available online 2 February 2008

Abstract

The use of Euler equations in Geophysics and Astrophysics is reviewed. Recent developments and new applications are emphasized. Examples are buoyancy columns in rotating fluids, possible preference for axisymmetric inertial convection at low Prandtl numbers, resonance properties of precessing spheroidal fluid filled cavities, and the possible absence of turbulence in rotating shear flows in the limit of high Reynolds numbers.

PACS: 47.10.A-; 47.15.ki; 47.20.Bp; 47.20.Qr; 47.32.-y; 97.10.Gz; 97.10.Kc; 97.25.Za

Keywords: Euler equations; Rotating fluids; Thermal Rossby waves; Inertial convection; Rotating stars; Precessing spheroids; Absence of turbulence; Bimodal convection

1. Introduction

Euler equations as well as their dissipative equivalent, the Navier–Stokes equations, have been applied to a large variety of problems in geophysics and astrophysics and through their use an impressive progress in the understanding of dynamical processes occurring in nature has been achieved. One of the not yet fully understood aspects of these applications is the close similarity between dynamical phenomena observed in the atmosphere and oceans and their pendants in laboratory experiments. This is surprising since the latter usually exhibit laminar flows, while their natural equivalents are fully turbulent. We shall return to this point at the end of this paper.

Fluid dynamics in geophysics and astrophysics is governed by actions of Coriolis and buoyancy forces. Euler equations for incompressible fluids seem to have even more applications in a rotating system than in a non-rotating system. This is caused by the property that in rotating fluids viscous dissipation is confined to thin layers attached to the solid boundaries, called Ekman layers, or to shear layers parallel to the axis of rotation, called Stewartson layers. The description of fluid flows can thus be simplified considerably in that the Euler equations govern the dynamics in the bulk of the fluid, while modifications caused by viscous friction can be treated as perturbations. We refer to Greenspan's [1] book for details on the various ways in which problems can be solved through expansions in powers of the Ekman number E. This parameter is defined with the kinematic viscosity ν of the fluid, the angular velocity Ω of rotation, and a typical length scale h of the system in the direction of the axis of rotation, $E = \nu/\Omega h^2$. E is usually rather small, say of the order 10^{-3} or less, in laboratory experiments with rotating fluids.

A second property of rotating systems that facilitates the description of dynamical processes on the basis of dissipationless equations is the possible balance between Coriolis and buoyancy forces. In contrast to non-rotating systems where simple equilibria can only be obtained when the hydrostatic balance, $\nabla\rho \times \nabla\Phi = 0$, is satisfied, a much wider variety of equilibria can be attained in rotating fluids in the form of the thermal wind balance,

$$2\boldsymbol{\Omega} \cdot \nabla \boldsymbol{v} = \nabla\rho \times \nabla\Phi. \tag{1}$$

Here $\boldsymbol{v}$ is the velocity field, ρ denotes the density distribution of the fluid and Φ is the potential of the force acting on it. Some examples for relationship (1) will be mentioned in the following.

Since the applications of Euler equations in geophysics and astrophysics go back nearly as far as their first publication in 1757, it is impossible to review all of them in a short article.

* Tel.: +49 0921 55 3329; fax: +49 0921 55 5820.
E-mail address: busse@uni-bayreuth.de.

0167-2789/$ - see front matter
doi:10.1016/j.physd.2008.01.024

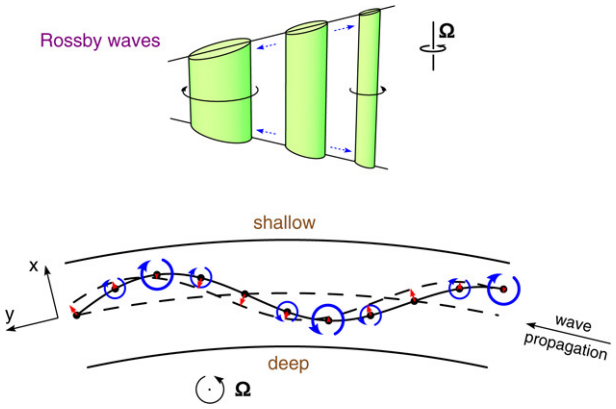

Fig. 1. Sketches for the dynamics of Rossby waves.

The use of Euler equations flourished in the 19th century when water waves were studied and the theory of the action of tides and of precession on rotating fluids was developed. A good access to these and other applications can be found in Lamb's [2] "Hydrodynamics". Modern books on geophysical and astrophysical fluid dynamics are those of (in alphabetical order) Cushman-Roisin [3], Ghil and Childress [4], Gill [5], McWilliams [6], Pedlosky [7], and Tassoul [8]. Most of these books deal with problems in shallow fluid layers such as those posed by the dynamics of oceans and of the atmosphere.

In the present paper we shall focus the attention on more general configurations which are applicable to the dynamics of the deep interiors of planets and stars. Some recent developments will be reviewed which are not yet well known and indeed are yet unpublished in parts. Magnetohydrodynamic applications will not be considered in this paper. For these we refer to the recent volume [9] and the book by Rüdiger and Hollerbach [10].

2. Thermal Rossby waves

The basic theorem of rotating fluid dynamics is the Proudman–Taylor theorem which states that steady small amplitude motions of a barotropic rotating fluid do not vary in the direction of the axis of rotation when viscous effects can be neglected. "Small amplitude" means in this connection that the vorticity of the motion is negligible in comparison to the rotation rate of the system. The Proudman–Taylor condition is a consequence of the complete balance between Coriolis force and pressure gradient. This balance is also called geostrophic balance since it holds in good approximation for the large scale motions in the Earth's atmosphere.

Two-dimensional fluid motions cannot often be accommodated in physical reality and motions are thus forced to become time dependent. In the simplest cases the motions assume the form of propagating Rossby waves. As indicated in Fig. 1, Rossby waves can be understood on the basis of the conservation of angular momentum. When a column of fluid (aligned with the axis of rotation) moves into a shallower place it becomes compressed and, because of the conservation of mass, its moment of inertia increases. To conserve angular momentum its rotation relative to an inertial system must decrease. Relative to the rotating system it thus acquires anticyclonic vorticity. The opposite process happens when the column moves into a deeper place where it gets stretched in the direction of the axis of rotation and acquires cyclonic vorticity.

In the annular fluid layer of Fig. 1 the depth decreases with increasing distance from the axis. A sinusoidal displacement of the initially static fluid columns leads to a flow structure in the form of vortices which tend to move the columns to new positions as indicated by the dashed line in the lower plot of the figure, i.e. the initial sinusoidal displacement propagates as a wave in the prograde direction. A retrograde propagation relative to the sense of rotation will be obtained when the depth of the annular layer increases with distance from the axis.

A dispersion relation for Rossby waves can be derived when the linearized Euler equations relative to a system rotating with the constant angular velocity $\boldsymbol{\Omega}$ are considered,

$$\frac{\partial}{\partial t}\boldsymbol{v} + 2\,\boldsymbol{\Omega}\times\boldsymbol{v} = -\nabla\pi, \tag{2a}$$

$$\nabla\cdot\boldsymbol{v} = 0. \tag{2b}$$

Assuming the small-gap limit of the annulus configuration we introduce a cartesian system of coordinates with the x-, y- and z-coordinates in the radial, azimuthal and axial directions, respectively. The velocity field can then be written in the form

$$\boldsymbol{v} = \nabla\psi(x,y)\times\boldsymbol{k}\exp\{\mathrm{i}\omega t\} + \cdots, \tag{3}$$

where $\boldsymbol{k}$ is the unit vector in the z-direction and the dots indicate higher-order contributions since the deviation from the Proudman–Taylor condition are assumed to be small. By taking the z-component of the curl of Eq. (2a) we obtain

$$-\mathrm{i}\omega\Delta_2\psi - 2\Omega\boldsymbol{k}\cdot\nabla v_z = 0 \tag{4}$$

where the two-dimensional Laplacian $\Delta_2 \equiv \frac{\partial^2}{\partial x^2} + \frac{\partial^2}{\partial y^2}$ has been introduced. After averaging Eq. (4) over the height h of the annulus and using the boundary conditions,

$$v_z \pm \eta\frac{\partial}{\partial y}\psi = 0 \quad \text{at } z = \pm h/2, \tag{5}$$

we find

$$-\mathrm{i}\omega\Delta_2\psi + \frac{4\Omega\eta}{h}\frac{\partial}{\partial y}\psi = 0. \tag{6}$$

The small parameter η is the tangent of the angle χ between the top boundary and the equatorial plane of the annulus. For simplicity the latter has been assumed as a plane of symmetry of the configuration as is also indicated in Fig. 2. The analysis of asymmetric configurations proceeds analogously since only the variation of the height in the direction of the axis of rotation matters.

A solution of Eq. (6) is easily obtained,

$$\psi(x,y) = \cos(\pi x/d)\exp\{\mathrm{i}\alpha y\}$$

$$\text{corresponding to } \omega = -\frac{4\Omega\eta\alpha}{h(\alpha^2 + (\pi/d)^2)}, \tag{7}$$

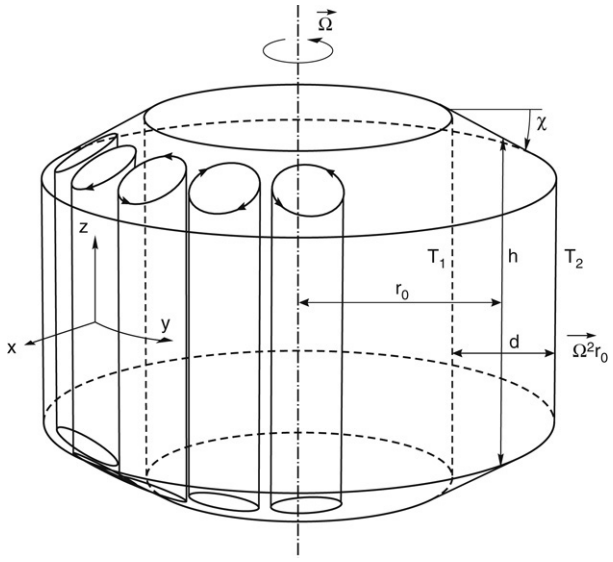

Fig. 2. Geometrical configuration of the rotating annulus.

which satisfies the boundary condition that the normal component of the velocity field vanishes at the side walls, $x = \pm d/2$, of the annulus.

Thermal Rossby waves are generated as growing disturbances when a temperature difference, $T_2 - T_1$, and a gravity force are applied in the x-direction such that a basic state with an unstable density stratification is obtained. The geometrical configuration is sketched in Fig. 2. In the experimental realization of the problem [11] the centrifugal force $\Omega^2 r_0$ is used as gravity and the temperature gradient must point outward in order to create the unstable density stratification. For geophysical applications one may think of the opposite directions for gravity and temperature gradient, but the mathematical problem is the same in both cases.

It is convenient to use a dimensionless description through the introduction of d as length scale, d^2/ν as time scale, and $(T_2 - T_1)/P$ as temperature scale where the Prandtl number P is defined as the ratio between kinematic viscosity ν and thermal diffusivity κ. The dimensionless equations for the streamfunction ψ and for the deviation Θ of the temperature from its static distribution assume the form

$$-\mathrm{i}\omega\Delta_2\psi + \eta^*\frac{\partial}{\partial y}\psi = R\frac{\partial}{\partial y}\Theta, \tag{8a}$$

$$\mathrm{i}\omega P\Theta + \frac{\partial}{\partial y}\psi = 0, \tag{8b}$$

where the Rayleigh number R and the dimensionless rotation parameter η^* are defined by

$$R = \frac{\gamma(T_2 - T_1)\Omega^2 r_0 d^3}{\nu\kappa}, \qquad \eta^* = \frac{4\Omega\eta d^3}{\nu h}. \tag{9}$$

Here γ denotes the coefficient of thermal expansion. In keeping with the philosophy of the Euler equations we have neglected the thermal diffusion term in the linearized heat equation (8b). Since the laboratory version of the problem has been chosen the higher temperature T_2 is assumed at the outer wall of the annulus. The solution for ψ of Eq. (8) has the same form as that of Eq. (6) while the expressions for Θ and ω are given by

$$\Theta = -\frac{\alpha\psi}{\omega P}\exp\{\mathrm{i}\omega t\} = -\cos(\pi x/d)\frac{\alpha}{\omega P}\exp\{\mathrm{i}\alpha y + \mathrm{i}\omega t\} \tag{10}$$

corresponding to

$$\omega_{1,2} = -\frac{\eta^*\alpha}{2(\alpha^2+\pi^2)} \pm \sqrt{\frac{(\alpha\eta^*)^2}{4(\pi^2+\alpha^2)^2} - \frac{R\alpha^2}{P(\pi^2+\alpha^2)}}. \tag{11}$$

In the limit $0 \le R \ll \eta^{*2}P/(\pi^2+\alpha^2)$ we recover the angular frequency of Rossby waves and in addition find the dispersion relation for a slow mode,

$$\omega_1 = -\frac{\eta^*\alpha}{(\alpha^2+\pi^2)}, \qquad \omega_2 = -\frac{R\alpha}{P\eta^*}. \tag{12}$$

In the case of the slow mode described by ω_2 the part of the Coriolis force that is not balanced by the pressure gradient is balanced by the buoyancy column Θ. As R increases the frequencies ω_1 and ω_2 move along the negative real axis in the complex ω-plane as indicated in Fig. 3. When R exceeds $\eta^{*2}P/4(\pi^2+\alpha^2)$, ω_1 acquires a negative imaginary part indicating a growing instability, called the thermal Rossby wave, while ω_2 corresponds to a decaying mode.

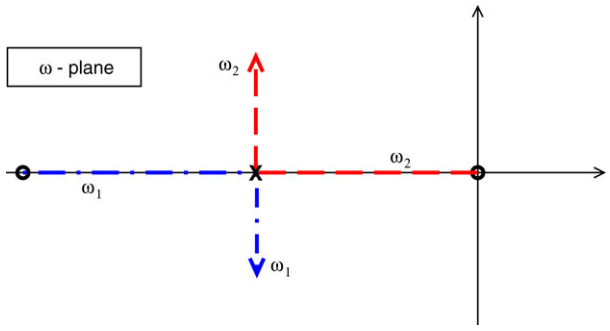

Fig. 3. Move in the complex ω-plane of the eigenvalues ω_1 and ω_2 with increasing R from their position at $R = 0$.

When dissipative terms are added in Eq. (8) all modes will decay except, possibly, the thermal Rossby wave. The critical value R_c of the Rayleigh number for the onset of the latter cannot be determined from Eq. (8) since it would correspond to an infinite α. When viscous friction and thermal diffusion are taken into account [12,13] the onset of thermal Rossby waves in the presence of stress-free walls is described by

$$R_c = \eta_P^{\frac{4}{3}}(3 + \pi^2\eta_P^{-\frac{2}{3}} + \cdots), \qquad \alpha_c = \eta_P^{\frac{1}{3}}(1 + \cdots),$$
$$\omega_c = -\sqrt{2}\eta_P^{\frac{2}{3}}(1 + \cdots)/P \quad \text{with } \eta_P \equiv \frac{\eta^* P}{\sqrt{2}(1+P)}. \tag{13}$$

This result describes in good approximation the onset of convection not only in rotating annuli, but in rotating fluid spheres as well [12] since only the azimuthal length scale described by α is important and the boundaries in the radial (i.e. perpendicular to the axis) direction do not enter the expressions in first approximation. For a more detailed discussion of the relationship between the analytical result (13) and numerical solutions for convection in rotating spheres see the recent review [14] where

also the relevance of the convection flows for the generation of planetary magnetic fields is discussed.

Here we want to return to the slow mode with its nearly stagnant buoyancy column. While it is damped in the simple annulus model, it becomes physically relevant when more than one source of buoyancy is admitted. In the Earth's core chemical buoyancy is released in the form of light elements in the neighborhood of the growing solid inner core and joins the thermal buoyancy in driving convection in the liquid outer core. This situation can be modeled in the rotating annulus configuration when a compositional gradient, $(C_2 - C_1)/d$, is added to the thermal gradient. A compositional Rayleigh number, C_R, can be defined in analogy to the definition (9) of R by replacing $\gamma(T_2-T_1)$ by $\gamma_C(C_2-C_1)$. The diffusion equation for the light elements is identical to the heat equation except that the Laplace operator is multiplied by the factor $1/L$ where L is the Lewis number. The latter denotes the ratio between thermal and compositional diffusivities and is assumed to be very large. In the limit $\frac{|C_R|\alpha}{P\eta^*} \ll 1$ the angular frequency of the slow mode and the corresponding value of the Rayleigh number R are given by [15],

$$\omega = -\frac{\alpha C_R}{P\eta^*}, \qquad R_c \approx \frac{(\pi^2+\alpha^2)^3}{\alpha^2} - \frac{P\omega^2(\pi^2+\alpha^2)}{\alpha^2}. \quad (14)$$

Since the last term can be neglected in the comparison with the preceding term, we recover the critical Rayleigh number for the onset of Rayleigh–Bénard convection in the absence of rotation! The buoyancy provided by the compositional gradient just serves to counteract the yet unbalanced portion of the Coriolis force. Note that this balance works independently of the sign of C_R. Please also note that the factor C_R/P is missing in the second term on the right-hand side in Eq. (13b) of [15].

3. Inertial waves and inertial convection

Inertial oscillations and waves represent an important class of solutions of the Euler equations in a rotating system. Axisymmetric solutions in containers that are symmetric with respect to the axis of rotation assume the form of standing oscillations, while non-axisymmetric solutions propagate in the form of waves. In contrast to Rossby waves which can be regarded as the quasi geostrophic subset of inertial waves and which propagate only in a single azimuthal direction, non-axisymmetric inertial waves may propagate in both azimuthal directions, albeit with different speeds. For an introduction to the theory of inertial waves we refer to Greenspan's [1] book. Among more recent results we like to mention the simplified representations of inertial waves in rotating spheres [16] and spheroids [17]. The theory of inertial oscillations is not only valid for incompressible fluids, but holds for barotropic fluids as well [18] and thus can be applied to the Sun and other stars. An unambiguous observational evidence for stellar inertial waves has not yet been obtained, however.

Slight modifications of inertial waves through the introduction of buoyancy and dissipative effects can lead to instabilities just as in the case of thermal Rossby waves. This property has been used by Zhang [19] and by Busse and Simitev [20] to obtain analytical solutions describing the onset of non-axisymmetric thermal convection in rotating spheres heated from within in the presence of a stress-free outer boundary. The corresponding problem with a no-slip outer boundary has been treated by Zhang [21]. We briefly study this problem here and describe some new results for axisymmetric inertial convection.

We consider a homogeneously heated, self-gravitating fluid sphere rotating with the constant angular velocity Ω about an axis fixed in space. A static state thus exists with the temperature distribution $T_S = T_0 - \beta r_0^2 r^2/2$ and the gravity field given by $\boldsymbol{g} = -\gamma_g r_0 \boldsymbol{r}$ where $\boldsymbol{r}$ is the position vector with respect to the center of the sphere and r is its length measured in fractions of the radius r_0 of the sphere. In addition to the length r_0, the time r_0^2/ν and the temperature $\nu^2/\gamma_g\gamma r_0^4$ are used as scales for the dimensionless description of the problem. The density is assumed to be constant except in the gravity term where its temperature dependence given by $\gamma \equiv -(\mathrm{d}\varrho/\mathrm{d}T)/\varrho = \text{const.}$ is taken into account. The basic equations of motion and the heat equation for the deviation Θ from the static temperature distribution are thus given by

$$\partial_t \boldsymbol{v} + \tau \boldsymbol{k} \times \boldsymbol{v} + \nabla\pi = \Theta \boldsymbol{r} + \nabla^2 \boldsymbol{v}, \quad (15a)$$

$$\nabla \cdot \boldsymbol{v} = 0, \quad (15b)$$

$$0 = R\boldsymbol{r} \cdot \boldsymbol{v} + \nabla^2\Theta - P\partial_t\Theta, \quad (15c)$$

where the Rayleigh number R, the Coriolis parameter τ and the Prandtl number P are defined by

$$R = \frac{\gamma\gamma_g\beta r_0^6}{\nu\kappa}, \qquad \tau = \frac{2\Omega r_0^2}{\nu}, \qquad P = \frac{\nu}{\kappa}. \quad (16)$$

We have neglected the nonlinear terms $\boldsymbol{v}\cdot\nabla\boldsymbol{v}$ and $\boldsymbol{v}\cdot\nabla\Theta$ in Eq. (15) since we restrict the attention to the problem of the onset of convection in the form of small disturbances. In the limit of high τ the right-hand sides of Eq. (15) can be neglected and the equation for inertial waves is obtained. For the description of inertial wave solutions $\boldsymbol{v}_0$ we use the general representation in terms of poloidal and toroidal components for the solenoidal field $\boldsymbol{v}_0$,

$$\boldsymbol{v}_0 = \nabla \times (\nabla(f\exp\{\mathrm{i}m\phi + \mathrm{i}\omega t\}) \times \boldsymbol{r}) + \nabla(g\exp\{\mathrm{i}m\phi + \mathrm{i}\omega t\}) \times \boldsymbol{r}, \quad (17)$$

where a spherical system of coordinates r, θ, ϕ has been introduced and f, g are functions of r and θ. By multiplying the $(\mathrm{curl})^2$ and the curl of the inertial wave equation by $\boldsymbol{r}$ we obtain two equations for f and g,

$$[\mathrm{i}\omega\mathcal{L}_2 - \mathrm{i}m\tau]\nabla^2 f - \tau\mathcal{Q}g = 0, \quad (18a)$$

$$[\mathrm{i}\omega\mathcal{L}_2 - \mathrm{i}m\tau]g + \tau\mathcal{Q}f = 0, \quad (18b)$$

where the operators $\mathcal{L}_2$ and $\mathcal{Q}$ are defined by

$$\mathcal{L}_2 \equiv (\sin\theta)^{-1}\partial_\theta(\sin\theta\,\partial_\theta) - m^2, \quad (19a)$$

$$\mathcal{Q} \equiv r\cos\theta\nabla^2 - (\mathcal{L}_2 + r\partial_r)(\cos\theta\,\partial_r - r^{-1}\sin\theta\,\partial_\theta). \quad (19b)$$

The only boundary condition to be satisfied by solutions of Eq. (18) is $f = 0$ at $r = 1$.

In the axisymmetric case $m = 0$ simple solutions of Eq. (18) can be found such as

$$f = P_1(r - r^3), \quad g = 2\mathrm{i}r^2\tau P_2/3\omega \quad \text{with } \omega = \pm\frac{\tau}{\sqrt{5}}, \tag{20a}$$

$$f = P_2(r^2 - r^4),$$
$$g = \mathrm{i}\tau\left(P_3\frac{4}{5}r^3 - 3P_1\left(r - \frac{7}{5}r^3\right)\right)\Big/\omega$$
$$\text{with} \quad \omega = \pm\tau\sqrt{\frac{3}{7}}, \tag{20b}$$

$$f = P_1\left(r - \frac{14}{5}r^3 + \frac{9}{5}r^5\right) + P_3(r^3 - r^5)\left(\frac{1}{5} - \frac{\omega^2}{\tau^2}\right)\frac{7}{3},$$
$$g = \mathrm{i}\left(P_2\left(\frac{28}{3}r^2 - 12r^4\right)\frac{\omega}{\tau} + P_4 r^4\left(\frac{2\tau}{5\omega} - \frac{2\omega}{\tau}\right)\right)$$
$$\text{with } \omega = \pm\tau\sqrt{\frac{1}{3} \pm \sqrt{\frac{4}{63}}}, \tag{20c}$$

where the functions $P_n = P_n(\cos\theta)$ are the Legendre polynomials. A typical property of inertial modes with $m = 0$ is that solutions always exist with both signs of ω such that they can be realized in the form of standing oscillations. This property contrasts with that of non-axisymmetric modes which always propagate in either the prograde or the retrograde direction, but with different speeds.

In order to solve the full Eq. (15) by the perturbation approach we first obtain an expression for Θ. Restricting attention to the limit $P\tau \ll 1$, but allowing for either a fixed temperature, $\Theta = 0$ at $r = 1$ (case A), or a thermally insulating boundary, $\partial\Theta/\partial r = 0$ at $r = 1$ (case B), we obtain

$$\Theta = P_l(\cos\theta)\exp\{\mathrm{i}\omega t\}h_l(r), \tag{21}$$

with

$$h_l(r) = l(l+1)R\left(\frac{r^{l+4}}{(l+5)(l+4) - (l+1)l} - \frac{r^{l+2}}{(l+3)(l+2) - (l+1)l} - cr^l\right), \tag{22}$$

where the coefficient c is given by

$$c = \begin{cases} \dfrac{1}{(l+5)(l+4) - (l+1)l} - \dfrac{1}{(l+3)(l+2) - (l+1)l}, \\ \dfrac{(l+4)/l}{(l+5)(l+4) - (l+1)l} - \dfrac{(l+2)/l}{(l+3)(l+2) - (l+1)l}, \end{cases} \tag{23}$$

in the cases A and B, respectively. The expressions (22) and (23) apply only for $l = 1$ and $l = 2$, i.e. for solutions (20a) and (20b). For solution (20c) and all other axisymmetric inertial oscillations more complex expressions must be expected.

When the perturbation expansion $\boldsymbol{v} = \boldsymbol{v}_0 + \boldsymbol{v}_1 + \cdots$ is inserted into Eq. (15a) it must be taken into account that the perturbation $\boldsymbol{v}_1$ consists of two parts, $\boldsymbol{v}_1 = \boldsymbol{v}_i + \boldsymbol{v}_b$ where $\boldsymbol{v}_i$ denotes the perturbation of the interior flow, while $\boldsymbol{v}_b$ is the Ekman boundary flow which is required because $\boldsymbol{v}_0$ does not satisfy the viscous boundary condition. Assuming a stress-free boundary we require

$$\boldsymbol{r}\cdot\nabla(\boldsymbol{r}\times(\boldsymbol{v}_0 + \boldsymbol{v}_b)/r^2) = 0 \quad \text{at } r = 1. \tag{24}$$

The solvability condition for the equation for $\boldsymbol{v}_1$ is obtained by multiplying it with $\boldsymbol{v}_0^*$ and averaging it over the fluid sphere,

$$0 = \langle\Theta\boldsymbol{r}\cdot\boldsymbol{v}_0^*\rangle + \langle\boldsymbol{v}_0^*\cdot\nabla^2(\boldsymbol{v}_0 + \boldsymbol{v}_b)\rangle, \tag{25}$$

where the brackets $\langle\cdots\rangle$ indicate the average over the fluid sphere and the $*$ indicates the complex conjugate. We have also anticipated that there is no perturbation contribution to the frequency since all terms in Eq. (25) are real. In the evaluation of the integrals in Eq. (25) the remarkable result that $\langle\boldsymbol{v}_0^*\cdot\nabla^2\boldsymbol{v}_0\rangle = 0$ holds for all inertial oscillations in rotating spheroidal cavities [17] can be used. Otherwise the evaluation proceeds as in Section 2 of [20] and yields in the case of solution (20a) the analytical expression

$$R = \frac{44\cdot(7\cdot5\cdot3)^2}{173 \mp 99} \approx 4169.4 \pm 2386.0, \tag{26}$$

where the upper sign applies in the case A and the lower sign in case B. For solution (20b) higher values of R are found in both cases and the same must be expected for all other axisymmetric solutions. Since the values (26) are only slightly larger than those obtained in [20] for non-axisymmetric inertial convection with $m = 1$ in the cases A and B, respectively, a close competition of the latter mode and convection in the form of the inertial oscillation (20a) must be expected at the onset of convection for sufficiently small values of $P\tau$. Indeed, numerical computations indicate that for intervals around $P\tau = 20$ and $P\tau = 5$ in the cases A and B, respectively, the axisymmetric mode sets in at a lower value of the Rayleigh number than all non-axisymmetric ones.

The axisymmetric convection described by the inertial wave (20a) corresponds to a flow along the axis of rotation from south to north in one phase of the cycle with a return flow along the surface which owing to the Coriolis force yields a retrograde (prograde) zonal flow in the northern (southern) hemisphere. The Coriolis force acting on this zonal flow in turn causes a reversal of the meridional circulation with the flow along the axis directed from north to south in the second half of the cycle. It will be of interest to find out whether such oscillations are realized in rotating stars.

4. Solutions of nonlinear Euler equations

4.1. Baroclinic rotating stars

Ever since von Zeipel [22] formulated his famous theorem that a hydrostatic equilibrium in rotating stars is not possible, the state of motion in axisymmetric rotating stars has been of considerable concern to astrophysicists. Vogt [23], Eddington [24], and later Sweet [25] assumed that low amplitude meridional circulations are realized, but it soon became apparent that those motions break down through the advection of angular momentum [26,8,27]. An alternative resolution of von Zeipel's paradox has been proposed by Schwarzschild [28], Roxburgh [29], and others who demonstrated that for a particular differential rotation

which depends only on the distance from the center the basic equations of stellar structure could be satisfied without meridional circulations. It seems unlikely, however, that such a special differential rotation could be attained from arbitrary initial angular momentum distributions. Here we want to draw attention to more general solutions of the Euler equations that can accommodate angular momentum distributions with arbitrary dependences on the distance from the axis.

To demonstrate the essential points we consider an idealized star with most of its mass concentrated in the core and its energy flux $\boldsymbol{F}$ dependent only on the temperature distribution such that

$$\Phi = -g_0 r_0^2/r \quad \text{and} \quad \boldsymbol{F} = f(T)\nabla T \tag{27}$$

can be assumed where r_0 is the radius of the star and g_0 is its surface gravity. In the absence of motion in an inertial system the hydrostatic equilibrium,

$$T = T^{(0)}(r), \qquad p = p^{(0)}(r), \qquad \rho = \rho^{(0)}(r), \tag{28}$$

is possible. In particular, it can be assumed that the boundary condition $T = \rho = 0$ for $p = 0$ is satisfied. Since we assume an ideal gas, $p/\rho = R_g T$ where R_g is the gas constant, solution (28) satisfies the relationship

$$\frac{1}{R_g T^{(0)}}\nabla\Phi = -\frac{1}{p^{(0)}}\nabla p^{(0)} = p^{(0)}\nabla\frac{1}{p^{(0)}}. \tag{29}$$

We anticipate that in the presence of a motion of the form $\boldsymbol{v} = \omega(r,\theta)\boldsymbol{k}\times\boldsymbol{r}$ with $\theta = \arccos(\boldsymbol{r}\cdot\boldsymbol{k}/r)$, where $\boldsymbol{k}$ denotes a constant unit vector, the thermodynamic variables can be written in the form

$$\begin{aligned} &T = T^{(0)}(r), \qquad p = p^{(0)} + p^{(1)}, \\ &\rho = (p^{(0)} + p^{(1)})/R_g T^{(0)}, \end{aligned} \tag{30}$$

where $p^{(1)}$ is not necessarily small in comparison to $p^{(0)}$. The nonlinear equation of motion now assumes the form

$$\begin{aligned} \rho\omega^2(\boldsymbol{k}\times\boldsymbol{r})\times\boldsymbol{k} &= \nabla p^{(1)} + \frac{p^{(1)}}{R_g T^{(0)}}\nabla\Phi \\ &= p^{(0)}\nabla\frac{p^{(1)}}{p^{(0)}} = p^{(0)}\nabla\frac{p^{(1)}+p^{(0)}}{p^{(0)}}, \end{aligned} \tag{31}$$

from which

$$\omega^2(\boldsymbol{k}\times\boldsymbol{r})\times\boldsymbol{k}/R_g T^{(0)} = \nabla\ln\frac{p^{(1)}+p^{(0)}}{p^{(0)}}, \tag{32}$$

follows. Necessary and sufficient for a solution $p^{(1)}$ of Eq. (31) is thus

$$\omega^2 = G(r\sin\theta)R_g T^{(0)}(r), \tag{33}$$

where the arbitrary function G is sufficient to accommodate all axisymmetric angular momentum distributions [27]. In the special case of a constant function G a purely r-dependent angular velocity ω is obtained as proposed by Schwarzschild [28] and Roxburgh [29].

In Fig. 4 a sketch for an example of the solution (33) is shown. Typically, the ellipticity of the isopycnals exceeds that of the isobars which in turn exceeds that of the isotherms.

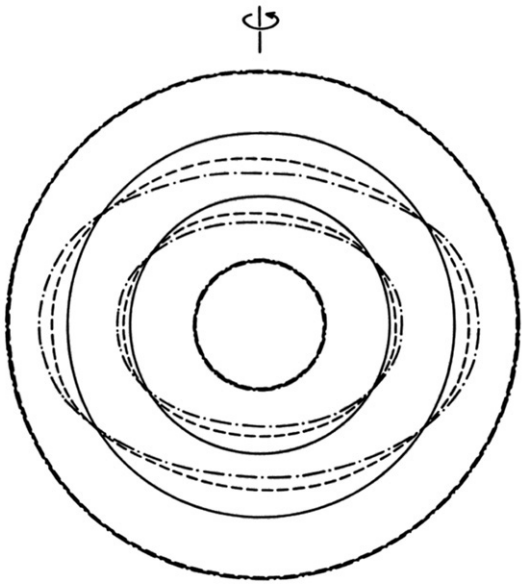

Fig. 4. Simple model of a rotating baroclinic star. Surfaces of constant temperature (solid lines), of constant pressure (dashed lines) and constant density (dash-dotted lines) are shown.

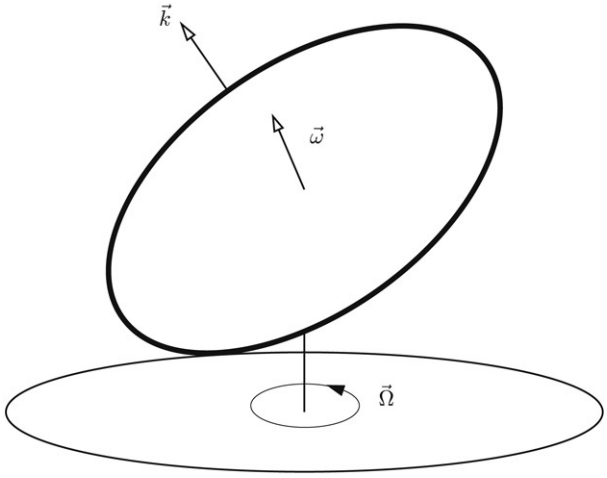

Fig. 5. Geometrical configuration of the precessing spheroidal cavity.

4.2. Flow in a precessing spheroidal cavity

The flow in a precessing spheroidal cavity is of considerable geophysical interest since it applies to the liquid core of the Earth. The solar–lunar precession of the Earth's axis of rotation about the normal of the ecliptic plane with a period of 25 700 years is a result of the torques exerted by Sun and Moon on the equatorial bulge of the Earth. The ellipsoidal flattening of the Earth's figure caused by the centrifugal potential is about 1/300. Owing to its higher density the ellipticity of the iron core is lower than that of the Earth's mantle. Hence the precessional torques exerted on the latter by Sun and Moon are larger than those acting on the core. There is thus an unbalanced precessional torque exerted by the mantle on the core. This situation can be modeled by a fluid filled spheroidal cavity rotating about its figure axis in a system that is rotating about a different axis as indicated in Fig. 5.

The Euler equations relative to the frame of reference precessing with the angular velocity $\boldsymbol{\Omega}$ (mantle frame) are given by

$$\partial_t \boldsymbol{v} + \boldsymbol{v}\cdot\nabla\boldsymbol{v} + 2\Omega\times\boldsymbol{v} + \nabla\pi = 0, \tag{34a}$$

$$\nabla\cdot\boldsymbol{v} = 0. \tag{34b}$$

The normal component of the velocity must vanish at the boundary of the spheroidal cavity,

$$\boldsymbol{v}\cdot(\boldsymbol{r} + \zeta\boldsymbol{k}\boldsymbol{r}\cdot\boldsymbol{k}) = 0 \quad \text{at} \quad |\boldsymbol{r}|^2 + \zeta|\boldsymbol{k}\cdot\boldsymbol{r}|^2 = 1, \tag{35}$$

where we have introduced the equatorial radius a of the cavity as length scale and where the parameter ζ is related to the ellipticity $\eta = (a-c)/a$ through $\zeta = \eta(2-\eta)/(1-\eta)^2$. The unit vector $\boldsymbol{k}$ indicates the figure axis of the cavity.

Sloudsky [30] and later independently Poincaré [31] derived a steady solution with constant vorticity for the problem (34) and (35),

$$\boldsymbol{v} = \boldsymbol{\omega}\times\boldsymbol{r} + \nabla\Psi \quad \text{with} \tag{36a}$$

$$\boldsymbol{\omega} = \boldsymbol{k}\cdot\boldsymbol{\omega}\left(\boldsymbol{k} + \boldsymbol{k}\times(\boldsymbol{\Omega}\times\boldsymbol{k})\frac{2+\zeta}{\zeta\boldsymbol{k}\cdot\boldsymbol{\omega} + 2\boldsymbol{k}\cdot\boldsymbol{\Omega}(1+\zeta)}\right), \tag{36b}$$

$$\Psi = \frac{\zeta\boldsymbol{k}\cdot\boldsymbol{r}\,(\boldsymbol{\Omega}\times\boldsymbol{k})\cdot\boldsymbol{r}\boldsymbol{k}\cdot\boldsymbol{\omega}}{\zeta\boldsymbol{k}\cdot\boldsymbol{\omega} + 2\boldsymbol{k}\cdot\boldsymbol{\Omega}(1+\zeta)}. \tag{36c}$$

There are two difficulties with this solution which occur also in other applications of the Euler equations:

- The vorticity component in the direction of $\boldsymbol{k}$ remains undetermined.
- The assumption of a constant vorticity vector in the interior may not be correct, even in the limit of vanishing viscosity.

The first of these difficulties can be resolved when the viscous Ekman layer is added to the solution (36). According to the analysis of Busse [32] the expression (36b) becomes

$$\boldsymbol{\omega} = \omega^2\left(\boldsymbol{k} + \boldsymbol{k}\times\frac{\boldsymbol{\Omega}2.62\sqrt{E\omega} + (\boldsymbol{\Omega}\times\boldsymbol{k})(\eta\omega^2 + \boldsymbol{k}\cdot\boldsymbol{\Omega} + 0.259\sqrt{E/\omega})}{(2.62\sqrt{E\omega})^2 + (\eta\omega^2 + \boldsymbol{k}\cdot\boldsymbol{\Omega} + 0.259\sqrt{E/\omega})^2}\right) \tag{37}$$

where $E = \nu/(a^2\omega_c)$ is the Ekman number. In addition to the length scale a we are using $1/\omega_c$ as time scale where ω_c is the angular velocity of the cavity. It has also been assumed that E, η, and $|\boldsymbol{\Omega}|$ are small quantities. Expression (37) agrees with the corresponding expression derived earlier by Stewartson and Roberts [33], but is correct in the order $\epsilon^2 \equiv 1-\omega^2$ instead of only in the order ϵ. In the limit $E \to 0$ and for small η and $|\boldsymbol{\Omega}|$ expression (37) agrees with expression (36b) with the implication $\omega^2 = \boldsymbol{k}\cdot\boldsymbol{\omega}$.

The assumption of a constant vorticity vector in the limit of vanishing viscosity has been established by the Prandtl–Batchelor theorem [34] in the case of a steady two-dimensional vortex, but this theorem cannot be extended to three-dimensional configurations in rotating systems even if the flow is essentially two-dimensional. In general tangential discontinuities and even divergences must be expected since they are admitted by the Euler equations. An example is the deviation from the Sloudsky–Poincaré solution (36) caused by the presence of the no-slip boundary as has been demonstrated by Busse [32]. In this latter paper it is shown that the flow of finite amplitude in the Ekman boundary layer causes a cylindrical shear layer in the interior of the precessing cavity at the distance $\sqrt{3}/2$ from the axis determined by $\boldsymbol{\omega}$ in the case of the sphere with the radius 1. This singularity is caused by the fact that the thickness of the Ekman boundary layer diverges like $\sqrt{E/|\boldsymbol{k}\cdot\boldsymbol{r}-\omega|}$ at the critical latitudes given by $\boldsymbol{k}\cdot\boldsymbol{r} = \omega$. In the case of a precessing sphere with $|\boldsymbol{k}-\boldsymbol{\omega}| \ll 1$ these latitudes are located at $\pm 30°$. A theoretical profile in the limit $E \to 0$ together with a profile measured in the experiment of Malkus [35] and a profile obtained by Noir et al. [36] in a numerical simulation with $E = 10^{-6}$ are shown in Fig. 6. A visualization of the shear layer in the case of an oblate spheroid can be seen in Fig. 7. To achieve a closer correspondence between the asymptotic profile and the other curves shown in Fig. 6 higher-order terms in the description of the Ekman layer near its divergence need to be taken into account in the asymptotic analysis.

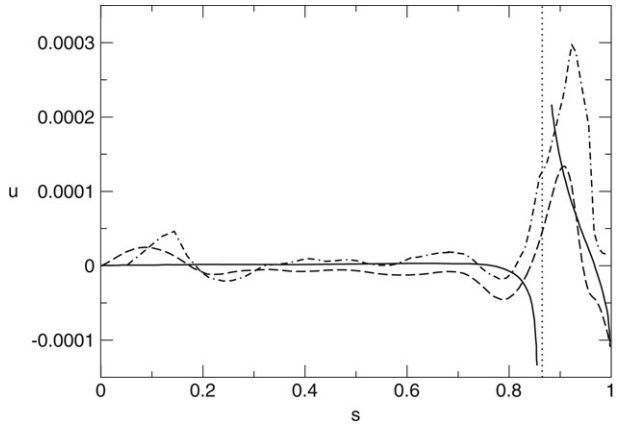

Fig. 6. Differential rotation in a precessing nearly spherical cavity as a function of the distance from the axis. Results of the asymptotic analysis [32] (solid lines) and from a numerical simulation for $E = 10^{-6}$ [36] (dashed line) are compared with the experimental measurement of Malkus [35] (dash-dotted line). The dotted line indicates the cylindrical surface intersecting the boundary at the critical latitudes.

The divergence of the Ekman layer at the critical latitudes also causes the excitation of inertial waves [37] which in turn spawn oscillatory internal shear layers which are oblique with respect to the rotation axis of the fluid [38,39]; see also [40,41]. With increasing amplitude of precession nonlinear effects of these shear layers give rise to interior differential rotations that are much more complex than that exhibited in Fig. 7; see, for example, the experimental photographs of [42].

Of special interest is the possibility of a resonance in expression (37) when $\boldsymbol{\Omega}\cdot\boldsymbol{k}$ is negative such that the denominator can approach zero in the limit $E \to 0$. Such a resonance represents the excitation of the inertial spin-over mode. But this inertial mode depends on the rotation vector of the fluid, not on the prescribed rotation of the container. Owing to the implicit nature of expression (37) for $\boldsymbol{\omega}$ there does not exist a simple linear resonance. Instead a complex nonlinear relationship in

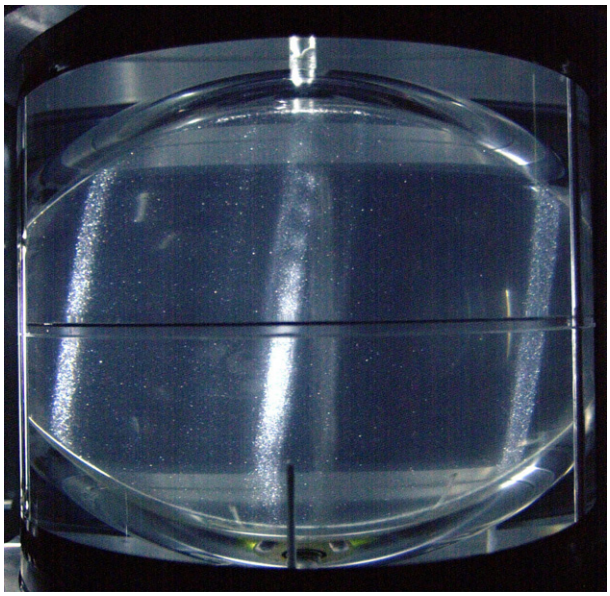

Fig. 7. Cylindrical shear layer in the precessing spherical cavity of the experiment of [43]. The shear becomes visible through the alignment of tiny flat particles. This photograph has been provided by the authors of [37]. A modified version of the figure has been published in [37].

the dependence of $\boldsymbol{\omega}$ admitting multiple solutions exist in the neighborhood of $\boldsymbol{\Omega} \cdot \boldsymbol{k} \approx -\eta$ as has been shown by Noir et al. [43]. These authors have investigated the resonance also experimentally and have found that expression (37) describes the measurements quite well even when the perturbation parameter ϵ approaches the order unity as shown in Figs. 7 and 9 of [43]. This is much beyond the range of small ϵ for which expression (37) had been derived originally. For a related discussion with respect to the experiments of Malkus [35] see [44].

5. The possible absence of turbulence in some shear flows for $Re \to \infty$

One of the most discussed problems in astrophysical fluid dynamics is the problem of turbulence in accretion disks. In the outer parts of the latter, where the electrical conductivity is too low for the Lorentz force to play a significant role, hydrodynamically generated turbulence is expected to be responsible for an efficient outward transport of angular momentum. This problem has focused the attention on the onset of turbulence in flows between two coaxial cylinders with radii r_1 and r_2 with $r_1 < r_2$ and associated constant angular velocities Ω_1 and Ω_2 with $\Omega_1 > \Omega_2 > 0$. According to Rayleigh's criterion the basic solution $\Omega(r)$ depending solely on the distance r from the axis is unstable with respect to axisymmetric disturbances when the condition

$$\frac{\mathrm{d}(r^2\Omega)}{\mathrm{d}r} < 0 \tag{38}$$

is satisfied. In the small-gap limit this criterion can be written in the form

$$\tau < Re \tag{39}$$

where the definitions

$$Re = \frac{(\Omega_1 - \Omega_2)d(r_2 + r_1)}{2\nu}, \qquad \tau = \frac{(\Omega_1 + \Omega_2)d^2}{\nu} \tag{40}$$

have been introduced with the gap width $d = r_2 - r_1$. Criterion (39) can be stated in a simple way: When shear vorticity and global vorticity have opposite signs, the former must exceed the latter in magnitude for instability.

Linear analysis of the stability with respect to infinitesimal disturbances confirms criterions (38) and (39) for instability at least for large values of Re. For lower values viscosity contributes a stabilizing influence such that the criterion for onset of infinitesimal disturbances in the small-gap limit becomes

$$Re > \frac{Re_E^2}{4\tau} + \tau \tag{41}$$

where R_E is the energy stability limit for plane Couette flow [45,46], $R_E = 2\sqrt{1708}$. Here the value 1708 refers to the well known critical value of the Rayleigh number for the onset of Rayleigh–Bénard convection in a horizontal fluid layer heated from below with no-slip boundaries. Experimental observations and numerical simulations based on the nonlinear Navier–Stokes equations agree with criterion (41) for the onset of instability – even if disturbances of finite amplitude are admitted – unless τ becomes small in comparison to R_E [47–49]. This does not exclude, however, the possibility of the existence of yet unrealized turbulent states of flow when the right-hand side of criterion (41) exceeds Re while τ is sufficiently large, say $\tau \gtrsim R_E/2$ is satisfied. A recent paper on bounds for the momentum transport in rotating systems considers this question [50].

It is a common notion among fluid dynamicists that all shear flows become turbulent provided the Reynolds number is sufficiently large and disturbances of finite amplitude are admitted. The absence of any turbulent flow under stationary conditions in the regime

$$-R_E \le Re \le \frac{Re_E^2}{4\tau} + \tau \tag{42}$$

as proposed in [50] contradicts this notion since Re can become arbitrarily large provided that τ becomes even larger. The proof for this proposal is incomplete, however, and is actually restricted to the neighborhood of $\tau = Re_E/2$ at which point the right-hand side of inequality (42) becomes equal to Re_E. If the proposal is correct, however, as is suggested by the presently available experimental and numerical evidence, then angular velocity distributions $\Omega(r)$ with $\mathrm{d}\Omega/\mathrm{d}r \le 0$ satisfying

$$\frac{\mathrm{d}(r^2\Omega)}{\mathrm{d}r} \ge 0 \tag{43}$$

are absolutely stable. Since the Keplerian velocity field in accretion disks is governed by the balance between

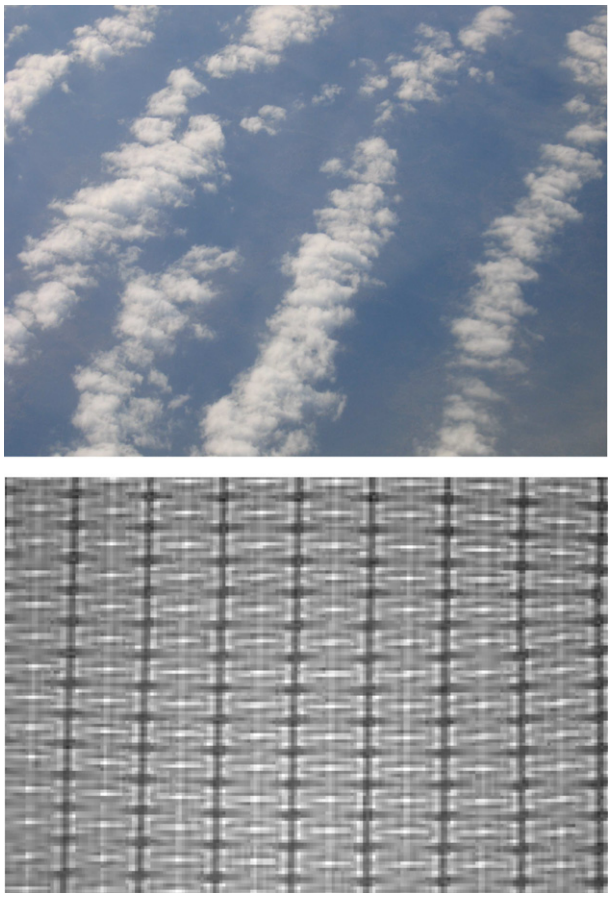

Fig. 8. Bimodal pattern in a cloud street (top, as seen from an airplane) and shadowgraph image of bimodal convection in a laboratory experiment (bottom, dark areas indicate rising hotter liquid, while bright areas indicate descending colder liquid; for further details see [56]).

gravitational attraction and the centripetal force, $\Omega^2 r \backsim 1/r^2$, it satisfies (43) and accretion disks cannot be turbulent under the idealized conditions considered here. In terms of the small-gap limit, $Re \approx d^2\nu^{-1}r|\mathrm{d}\Omega/\mathrm{d}r| \approx \Omega 3d^2/2\nu \approx 3\tau/4$ grows only in proportion to $3\tau/4$ asymptotically and thus cannot give rise to turbulence according to criterion (42).

Of course, hydrodynamic turbulence in accretion disks could be generated through additional effects such as a stable density stratification in the direction normal to the disk. Theoretical analyses [51–53] confirmed by recent experimental work [54] support this idea in that they demonstrate that in a Taylor–Couette system an axisymmetric density gradient in the direction of gravity exerts a destabilizing influence on the onset of instability such that Rayleigh's criterion (38) is violated.

6. Bimodal convection in geophysics

In order to illustrate the close similarity between laboratory flows and corresponding observed geophysical phenomena we choose the case of bimodal convection since it is not as well known as other examples such as von Karman vortex streets in the wake of some oceanic islands, Kelvin–Helmholtz waves in the atmosphere, or cloud patterns corresponding to convection rolls and hexagonal cells. Bimodal convection originates from an instability of convection rolls and is driven by the buoyancy stored in the thermal boundary layers associated with a convecting fluid layer [55]. It has been studied experimentally by Busse & Whitehead [56] and its finite amplitude properties have been analyzed numerically by Frick et al. [57]. A laboratory shadowgraph image is shown in Fig. 8 together with an observed example of bimodal structures in a cloud street. Another observational example can be found in the recent review [58]. This agreement between a laboratory convection pattern and an atmospheric phenomenon is remarkable in that bimodal convection is generated through a secondary bifurcation in contrast to the other examples mentioned above which correspond to primary bifurcations.

Since bimodal convection is usually observed only in fluids with a Prandtl number P in excess of the order 10, it may be surprising to observe this phenomenon in the atmosphere as air is characterized by a Prandtl number of only 0.7. It must be kept in mind, however, that the condensation of water vapor not only acts as a convenient indicator of upward motions, but also influences the thermodynamics of the convecting layer. The latent heat liberated through the condensation of water droplets causes an increase in the specific heat of the fluid which in turn lowers the effective thermal diffusivity. Since P is defined as the ratio of kinematic viscosity to thermal diffusivity it assumes a high value for convection in the presence of clouds.

Another case of bimodal convection may be found in the Earth's mantle. Convection cells involving the whole mantle are believed to be responsible for plate tectonics, i.e. for the motion of crustal plates in the outermost region of the "solid" Earth. Secondary motions beneath the plates appear to occur in many places as has been pointed out by Richter [59] and others. As in the case of laboratory bimodal convection (see Fig. 8) the smaller secondary convection rolls are always oriented at right angles to the larger primary convection rolls. In this way the stabilizing effect of the shear of the primary convection rolls on the secondary rolls is minimized. In the case of the Earth's mantle additional influences on convection arise, of course, from the presence of the olivine–spinel and the spinel–perovskite phase transitions at the depths of 400 km and 660 km, respectively.

7. Concluding remarks

In this review we have pointed out a few solutions of the Euler equations which have been of recent interest in the field of geophysical and astrophysical fluid dynamics. These simple solutions can be realized in laboratory experiments and also be applied to large scale fluid dynamical phenomena in geophysics and astrophysics. The fact that the latter systems are usually in a turbulent state of motion does not seem to affect the usefulness of the laminar solutions. Since the interaction of the large scale components of the velocity and buoyancy fields occurs rather independently of the influence of the small scale motions, the latter can roughly be taken into account as diffusive effects. From this point of view it is not surprising that the employment of eddy diffusivities has been quite successful in describing the effects of turbulence in geophysical and astrophysical systems.

Acknowledgments

The help of Drs. R. Simitev and T. Pöschel in creating the figures is gratefully acknowledged.

References

[1] H.P. Greenspan, The Theory of Rotating Fluids, Cambridge University Press, 1968.
[2] H. Lamb, Hydrodynamics, Dover Publications, 1945.
[3] B. Cushman-Roisin, Introduction to Geophysical Fluid Dynamics, Prentice-Hall, 1994.
[4] M. Ghil, S. Childress, Topics in geophysical fluid dynamics, in: Dynamo Theory and Climate Dynamics, Springer Verlag, 1987.
[5] A.E. Gill, Atmosphere-Ocean Dynamics, Academic Press, 1982.
[6] J.C. McWilliams, Fundamentals of Geophysical Fluid Dynamics, Cambridge University Press, 2007.
[7] J. Pedlosky, Geophysical Fluid Dynamics, 2nd ed., Springer Verlag, 1987.
[8] J.-L. Tassoul, Theory of Rotating Stars, Princeton University Press, 1968.
[9] E. Dormy, A.M. Soward (Eds.), Mathematical Aspects of Natural Dynamos, CRC Press, Taylor & Francis Group, 2007.
[10] G. Rüdiger, R. Hollerbach, The Magnetic Universe, Wiley-VHC, Weinheim, 2004.
[11] F.H. Busse, C.R. Carrigan, Laboratory simulation of thermal convection in rotating planets and stars, Science 191 (1976) 81–83.
[12] F.H. Busse, Thermal instabilities in rapidly rotating systems, J. Fluid Mech. 44 (1970) 441–460.
[13] F.H. Busse, Asymptotic theory of convection in a rotating, cylindrical annulus, J. Fluid Mech. 173 (1986) 545–556.
[14] F.H. Busse, Convective flows in rapidly rotating spheres and their dynamo action, Phys. Fluids 14 (2002) 1301–1314.
[15] F.H. Busse, Is low Rayleigh number convection possible in the Earth's core? Geophys. Res. Letts. 29 (2002) GLO149597.
[16] K. Zhang, P. Earnshaw, X. Liao, F.H. Busse, On inertial waves in a rotating fluid sphere, J. Fluid Mech. 437 (2001) 103–119.
[17] K. Zhang, X. Liao, P. Earnshaw, On inertial waves in a rapidly rotating spheroid, J. Fluid Mech. 504 (2004) 1–40.
[18] F.H. Busse, K. Zhang, X. Liao, On slow inertial waves in the solar convection zone, Astrophys. J. 631 (2005) L171–L174.
[19] K. Zhang, On coupling between the Poincaré equation and the heat equation, J. Fluid Mech. 268 (1994) 211–229.
[20] F.H. Busse, R. Simitev, Inertial convection in rotating fluid spheres, J. Fluid Mech. 498 (2004) 23–30.
[21] K. Zhang, On coupling between the Poincaré equation and the heat equation: No-slip boundary condition, J. Fluid Mech. 284 (1995) 239–256.
[22] H. von Zeipel, Probleme der Astronomie (Festschrift für H. von Seeliger), Springer-Verlag, Berlin, 1924, pp. 144–152.
[23] H. Vogt, Zum Strahlungsgleichgewicht der Sterne, Astron. Nachr. 223 (1925) 229–232.
[24] A.S. Eddington, Circulating currents in rotating stars, The Observatory 48 (1925) 73–75.
[25] P.A. Sweet, The importance of rotation in stellar evolution, Month. Not. Roy. Astron. Soc. 110 (1950) 548–558.
[26] G. Randers, Large-scale motions in stars, Astrophys. J. 94 (1941) 109–123.
[27] F.H. Busse, On the problem of stellar rotation, Astrophys. J. 259 (1982) 759–766.
[28] M. Schwarzschild, On stellar rotation. II, Astrophys. J. 106 (1947) 427–456.
[29] I.W. Roxburgh, On stellar rotation: I. The rotation of upper main-sequence stars, Month. Not. Roy. Astron. Soc. 128 (1964) 157–171.
[30] T. Sloudsky, De la rotation de la terre supposée a son intérieur, Bull. Soc. Impér. Natur. 9 (1895) 285–318.
[31] H. Poincaré, Sur la précession des corps déformables, Bull. Astr. 25 (1910) 321–356.
[32] F.H. Busse, Steady fluid flow in a precessing spheroidal shell, J. Fluid Mech. 33 (1968) 739–751.
[33] K. Stewartson, P.H. Roberts, On the motion of a liquid in a spheroidal cavity of a precessing rigid body, J. Fluid Mech. 17 (1963) 1–20.
[34] G.K. Batchelor, Steady laminar flow with closed streamlines at large Reynolds numbers, J. Fluid Mech. 1 (1956) 177–190.
[35] W.V.R. Malkus, Precession of the Earth as the cause of geomagnetism, Science 160 (1968) 259–264.
[36] J. Noir, D. Jault, P. Cardin, Numerical study of the motions within a slowly precessing sphere at low Ekman number, J. Fluid Mech. 437 (2001) 283–299.
[37] J. Noir, D. Brito, K. Aldridge, P. Cardin, Experimental evidence of inertial waves in a precessing spheroidal cavity, Geophys. Res. Lett. 28 (2001) 3785–3788.
[38] R.R. Kerswell, On the internal shear layers spawned by the critical regions in oscillatory Ekman boundary layers, J. Fluid Mech. 289 (1995) 311–325.
[39] R. Hollerbach, R.R. Kerswell, Oscillatory internal shear layers in rotating and precessing flows, J. Fluid Mech. 289 (1995) 327–339.
[40] A. Tilgner, Driven inertial oscillations in spherical shells, Phys. Rev. E 59 (1999) 1789–1794.
[41] M. Rieutord, B. Georgeot, L. Valdettaro, Inertial waves in a rotating spherical shell: Attractors and asymptotic spectrum, J. Fluid Mech. 435 (2001) 103–144.
[42] J. Vanyo, P. Wilde, P. Cardin, P. Olson, Experiments on precessing flows in the Earth's liquid core, Geophys. J. Int. 121 (1995) 136–142.
[43] J. Noir, P. Cardin, D. Jault, J.-P. Masson, Experimental evidence of non-linear resonance effects between retrograde precession and the tilt-over mode within a spheroid, Geophys. J. Int. 154 (2003) 407–416.
[44] S. Lorenzani, A. Tilgner, Inertial instabilities of fluid flow in precessing spheroidal shells, J. Fluid Mech. 492 (2003) 363–379.
[45] F.H. Busse, Über notwendige und hinreichende Kriterien für die Stabilität von Strömungen, ZAMM 50 (1970) T173–T174.
[46] F.H. Busse, A Property of the Energy Stability Limit for Plane Parallel Shear Flow, Arch. Ration. Mech. Anal. 47 (1972) 28–35.
[47] B. Dubrulle, O. Dauchot, F. Daviaud, P:-Y. Longaretti, D. Richard, J.-P. Zahn, Stability and turbulent transport in rotating shear flows: Prescription from analysis of cylindrical and plane Couette flows data, Phys. Fluids 17 (2005) 095103.
[48] H. Ji, M. Burin, E. Schartman, J. Goodman, Hydrodynamic turbulence cannot transport angular momentum effectively in astrophysical disks, Nature 444 (2006) 343–346.
[49] F. Rincon, G.I. Ogilvie, C. Cossu, On self-sustaining processes in Rayleigh-stable rotating plane Couette flows and subcritical transition to turbulence in accretion disks, Astron. Astrophys. 463 (2007) 817–832.
[50] F.H. Busse, Bounds on the momentum transport by turbulent shear flow in rotating systems, J. Fluid Mech. 583 (2007) 303–311.
[51] M.J. Molemaker, J.C. McWilliams, I. Yavneh, Instability and equilibration of centrifugally stable stratified Taylor–Couette flow, Phys. Rev. Lett. 86 (2001) 5270–5273.
[52] I. Yavneh, J.C. McWilliams, M.J. Molemaker, Non-axisymmetric instability of centrifugally stable stratified Taylor–Couette flow, J. Fluid Mech. 448 (2001) 1–21.
[53] D. Shalybkov, G. Rüdiger, Stability of density-stratified viscous Taylor–Couette flows, Astron. Astrophys. 438 (2005) 411–417.
[54] M. Le Bars, P. Le Gal, Experimental analysis of the stratorotational instability in a cylindrical Couette flow, Phys. Rev. Lett. 99 (2007) 064502.
[55] F.H. Busse, On the stability of two-dimensional convection in a layer heated from below, J. Math. Phys. 46 (1967) 140–150.
[56] F.H. Busse, J. Whitehead, Instabilities of convection rolls in a high-Prandtl number fluid, J. Fluid Mech. 47 (1971) 305–320.
[57] H. Frick, F.H. Busse, R.M. Clever, Steady three-dimensional convection at high Prandtl numbers, J. Fluid Mech. 127 (1983) 141–153.
[58] F.H. Busse, The Sequence-of-bifurcations approach towards understanding turbulent fluid flow, Surv. Geophys. 24 (2003) 269–288.
[59] F.M. Richter, Convection and the large-scale circulation of the mantle, J. Geophys. Res. 78 (1973) 8735–8745.